Structural Durability & Health Monitoring

Tech Science Press

https://doi.org/10.32604/sdhm.2026.083733

ARTICLE

Investigation of Early-Age Freeze-Thaw-Induced Damage Evolution in UHPC and the Structural Strengthening Efficacy of CFRP Systems

Yongbing Sun[1], **Dewen Liu**[1,2,*], **Qian Wang**[1,*], **Yuexia Yang**[3] **and Canhuan Pan**[3]

[1]College of Civil Engineering, Southwest Forestry University, Kunming, China
[2]International College, Krirk University, Bangkok, Thailand
[3]Yunnan Chutian Engineering Inspection Co., Ltd., Kunming, China

*Corresponding Authors: Dewen Liu. Email: civil_liudewen@sina.com; Qian Wang. Email: 99tmwangqian@swfu.edu.cn

Received: 09 April 2026; Accepted: 08 June 2026; Published: 23 October 2026

ABSTRACT: During winter construction in cold regions, ultra-high performance concrete (UHPC) is susceptible to early-age freeze-thaw cycles caused by improper curing or sudden cold waves. This study investigates the damage evolution of UHPC under freeze-thaw cycles and the subsequent strengthening effect of carbon fiber reinforced polymer (CFRP). Early-age (7-day cured) UHPC specimens were subjected to coupled freeze-thaw and chloride salt (5% NaCl) exposure. Damage was characterized by ultrasonic wave velocity, compressive strength, and SEM-EDS analysis. Results show that as the number of freeze-thaw cycles increases, mass loss reaches 1.35% at 150 cycles, while wave velocity decreases by 1.14%. Control specimens (without freeze-thaw) exhibited a 24.6% increase in compressive strength with age (corresponding to 150 cycles), whereas the strength of specimens subjected to 150 cycles decreased by 19.9%. After CFRP strengthening, the ratio η (strength of strengthened specimens to that of unstrengthened control specimens of the same age) declines with increasing cycles. The ratio α (strength of strengthened damaged specimens to that of unstrengthened damaged specimens of the same age) reaches 113.1% at 150 cycles, a 3.60% decrease from its initial value, indicating that more severe freeze-thaw damage leads to lower reinforcement efficiency. Microscopic analysis reveals that after 150 cycles, the chloride ion content reaches 0.3 wt%, steel fibers corrode, and the number of pores and microcracks increases. Meanwhile, the Ca/Si atomic ratio decreases due to calcium ion leaching and secondary hydration of silica fume. This study elucidates the evolution mechanism of early-age freeze-thaw damage in UHPC and validates the effectiveness of CFRP strengthening, providing a practical basis for the protection and retrofitting of UHPC structures in cold regions.

KEYWORDS: UHPC; early-age freeze-thaw cycling; carbon fiber–reinforced polymer (CFRP) strengthening; microstructural evolution

1 Introduction

Ultra-high performance concrete (UHPC) is a building material with great development potential, which is favored for its outstanding strength, durability and good workability. UHPC has an extremely low water-cement ratio and is usually made up of a large amount of cement, active mineral admixtures, well-graded fine aggregates, steel fibers and high-performance water reducers [1–3]. In the current construction field, UHPC structures are widely used. However, in winter construction in cold regions, UHPC structures often suffer from early-age freeze-thaw cycles due to improper curing or sudden cold waves. In cold areas, freeze-thaw cycles are a dominant factor leading to the deterioration of concrete structures. UHPC, with

Copyright © 2026 The Authors. Published by Tech Science Press. This work is licensed under a Creative Commons Attribution 4.0 International License, which permits unrestricted use, distribution, and reproduction in any medium, provided the original work is properly cited.

its extremely low porosity and dense microstructure, theoretically has excellent freeze-thaw resistance, but there are certain potential risks for early-age UHPC.

Regarding the definition of the early age of UHPC, there is no unified standard in the academic community at present, and it usually varies according to the research purpose and the development law of material properties. From the perspective of mechanical property development, the compressive strength of UHPC can reach over 70 MPa within 24 h after pouring [4], and its strength develops rapidly. Therefore, based on the existing research, the early age of UHPC generally refers to the critical stage from 1 to 28 d after pouring, during which the microstructure forms and the properties develop rapidly [5], while the period after 28 d is regarded as the mature stage of UHPC. During the early age, the degree of hydration, microstructure evolution and shrinkage behavior of the material will directly affect the later mechanical and durability properties of UHPC.

Existing research findings suggest that UHPC after 28 d of curing has excellent freeze-thaw resistance, and its strength may even increase due to the secondary hydration of unhydrated materials after freeze-thaw cycles [6]. However, research on the damage evolution law of early-age UHPC under freeze-thaw cycles is still limited (Liu et al. [7]). The shear performance of the UHPC-NC interface with planted reinforcement under freeze-thaw cycles was investigated, including 0, 20, 40, 60, 80, and 100 freeze-thaw cycles. It was found that after 100 cycles in a 3.5% salt solution environment, the interface shear strength decreased by 35%. Chi et al. [8] investigated the dynamic compressive performance of UHPC after extreme low-temperature (−160°C) freeze-thaw cycles. SEM analysis revealed that the freeze-thaw cycles led to gradual deterioration of the UHPC matrix and the fiber-matrix interface. After 8 freeze-thaw cycles, the calcium silicate hydrate (C-S-H) structure was further damaged, and obvious cracks appeared at the interface of steel fibers and cement matrix These studies indicate that UHPC itself has excellent freeze resistance, but microstructure damage can still occur under extreme or long-term freeze-thaw conditions.

Liu et al. [9] degradation of interface bonds in UHPC-NC composite materials during seawater freeze-thaw cycles was investigated, taking into account interface treatment and matrix NC strength grade. The results showed that the initial shear strength was highest for grooved interfaces, but they experienced severe deterioration, losing 44.2% after 75 cycles. Hao et al. [10] investigates the durability of recycled aggregate concrete under the coupled action of freeze-thaw cycles and flexural loading. The results show that with the increase of load ratio, microcracks increase significantly, the damage accumulation in the interfacial transition zone (ITZ) is aggravated, and the mechanical properties deteriorate rapidly. Mészöly et al. [11] investigated the flexural behavior of UHPC plates reinforced by the combination of fiber and textile reinforcement. The combination of high performance materials UHPC and carbon reinforcement creates structural elements with high efficiency and durability. Peng et al. [12] investigated the durability of UHPC repair materials under the combined action of chloride, sulfate, freeze-thaw and dry-wet cycles. The results indicate that the mixture incorporating 10% silica fume, 1% nucleating agent and 1.5% steel fibers exhibits the optimal comprehensive durability. Zhong et al. [13] investigated the chloride ion transport law and microstructure evolution of UHPC with initial microcracks under the coupling effect of freeze-thaw cycles and chloride ion erosion. The results indicated that freeze-thaw damage would accelerate chloride ion penetration. Weng et al. [14] used a micro-mechanical-based finite element method combined with X-ray computed tomography (CT) technology to establish a real microstructure geometric model, which fully considered the effects of curing age and freeze-thaw cycles on UHPC. Banik et al. [15] tested the freeze-thaw durability of pre-cracked UHPC specimens with different fiber types and fiber contents. The results show that pre-cracked UHPC presents self-healing and crack closure behaviors under freeze-thaw exposure and saturated conditions, as determined by resonant frequency measurement.

The above-mentioned research indicates that early-age UHPC will suffer significant damage accumulation under harsh freeze-thaw cycles, which is manifested as the generation of micro-cracks, deterioration of pore structure, and attenuation of macroscopic mechanical properties. For damaged concrete structures, taking effective reinforcement measures is the key to restoring their load-bearing capacity and extending their service life. Carbon fiber reinforced polymer (CFRP) composites feature light weight, superior strength, high modulus and great heat resistance. Owing to these merits, they are highly effective for strengthening UHPC members and have gained extensive application in civil engineering structural rehabilitation [16–19].

Peng et al. [20] studied the mechanical properties of CFRP-confined recycled aggregate concrete under the combined effects of sulfate corrosion and freeze-thaw cycles, confirming that CFRP can effectively improve the residual bearing capacity in freeze-thaw environments. Feng et al. [21] investigated the axial compressive performance of CFRP-confined concrete columns under different numbers of freeze-thaw cycles (0–125) and CFRP layers (0–3 layers), and established a bearing capacity prediction model considering the effects of freeze-thaw. Zhang et al. [22] explored the interfacial failure mechanism of CFRP-strengthened concrete under various erosive environments. It is found that higher wind speed of wind-sand erosion can raise the surface roughness of concrete, which effectively improves the bonding performance at the CFRP-concrete interface and elevates the peak stress level. Wang et al. [23] conducted a systematic study on how CFRP sheet thickness and UHPC affect the axial compression behavior of core concrete. It is found that benefiting from the synergistic confinement of CFRP and UHPC, the initial stiffness of composite reinforced specimens is 10%–16.4% higher than that of specimens strengthened only with UHPC. Che et al. [24] studied the seismic behavior of corroded RC columns strengthened with ECC and CFRP composite materials. It is demonstrated that the ductility coefficient of corroded reinforced concrete columns is improved by 34.13% when adopting ECC/CFRP combined strengthening, in contrast to single ECC reinforcement. Xu and Huang [25] conducted cyclic loading tests on short columns of corroded reinforced concrete strengthened with CFRP. The results showed that the after CFRP strengthening, their performance was significantly improved, even surpassing that of the un-corroded specimens. By adopting four-point bending tests coupled with acoustic emission (AE) monitoring, Jiang et al. [26] explored crack growth characteristics, failure patterns and mechanical behavior based on fracture mechanics theory.

Therefore, the present work systematically explores the damage development of early-age UHPC subjected to freeze-thaw action at cycle numbers of 0, 30, 60, 90, 120 and 150. Herein, 0 cycles correspond to the initial samples with a 7-day curing age. After 7 days, there is very little free water, and pure water causes almost no damage [27]. However, 5% NaCl generates osmotic pressure, driving the penetration of water/chloride ions, increasing freezeable water and corroding fibers, forming a freeze-thaw cracking cycle of deterioration. A key innovation is the elucidation of the macroscopic performance degradation and microscopic structural evolution mechanism of early-age UHPC subjected to freeze-thaw cycles. In addition, after each cycle node, damaged specimens were strengthened with externally bonded circumferential CFRP sheets. Another innovation is the proposal of a dual evaluation system for CFRP reinforcement effectiveness, in which η (strength recovery ratio) and α (reinforcement efficiency coefficient) are adopted to quantify the strengthening effect.

2 Experimental Materials and Schemes

2.1 Experimental Materials and Parameters

All UHPC specimens in the test were fabricated with commercial ready-mixed raw materials supplied by Zhongde Xinya Building Materials Co, Ltd. The raw materials are composed of fine quartz sand as aggregate, Portland cement, fly ash, silica fume and quartz powder as cementitious components, together with polycarboxylate superplasticizer as chemical admixture. meeting the standard performance requirements

of UHPC as stipulated in ASTM C1856 [28]. The designed reference strength of UHPC was C120. When pouring the UHPC specimens, 9% by weight of copper-coated steel fibers [29] and 9 ± 1% of water were added to the premixed materials. To prevent the steel fibers from rusting during long-term freeze-thaw cycles and affecting the mechanical properties of UHPC and the subsequent reinforcement effect, copper-coated steel fibers with a length of 13 mm were used in this study. The appearance and morphology of the copper-coated steel fibers are shown in Fig. 1, and their physical properties are listed in Table 1. The appearance and morphology of the CFRP used for reinforcement in this study are shown in Fig. 2, and its physical properties are listed in Table 2. The specimens were bonded with the matching carbon fiber impregnating adhesive. The experimental design mainly considered two parameters: the number of freeze-thaw cycles (0, 30, 60, 90, 120, and 150 times) and whether CFRP reinforcement was applied.



(**a**) Appearance and form (**b**) Size

Figure 1: Appearance and morphology of copper-coated steel fibers.

Table 1: Physical properties of copper-coated steel fibers.

Fiber Type	Length (mm)	Diameter (mm)	Tensile Strength (MPa)
Copper-plated steel fiber	13.00	0.20	2380



Figure 2: CFRP for reinforcement.

Table 2: Physical properties of CFRP.

Product	Gram Weight (g/m^2)	Theoretical Thickness (mm)	Tensile Strength (MPa)	Elastic Modulus (GPa)
CFRP	200	0.111	≥3000	≥210

2.2 Preparation of UHPC Test Blocks

The mixture proportions of raw materials for the prepared UHPC specimens are presented in Table 3.

Table 3: Mix proportions (kg/m^3).

Material	UHPC Premixed Material	Copper-Plated Steel Fiber	Water
Dosage	2500	225	250

The preparation process of UHPC specimens is shown in Fig. 3. During the UHPC mixing process, the premixed materials and steel fibers are first put into a horizontal mixer and mixed for 90 s, then water is added and mixed for 240 s. At this stage, a well-flowing UHPC slurry is formed, with the steel fibers randomly arranged throughout the mixing process. Subsequently, the UHPC matrix is poured into a 100 mm × 100 mm × 100 mm plastic mold. The mixture is vibrated for 20 s on a concrete vibrating table to ensure full compaction. Finally, a film is covered on the prepared mold (the surface of the mixture), and after 24 h, the specimens are demolded and placed in a standard curing room with a constant temperature of 20 ± 2°C and a relative humidity of 95% for 7 d. After the curing period, freeze-thaw cycle tests are conducted.



Figure 3: Specimen preparation process.

For each test, samples were taken after the cycles, as well as samples naturally cured for the time corresponding to the cycles. Specimens of the same age were used to eliminate the effects of natural aging; the difference between the freeze-thaw group and the same-age control group represents pure freeze-thaw damage.

2.3 Test Scheme for Early Age Freeze-Thaw Cycles

To accurately reflect the long-term service conditions of UHPC components under freeze-thaw cycles, this study selected NaCl solution as the medium for freeze-thaw cycles. The average annual mass fraction of chloride ions in seawater is approximately 1.49% [30]. In order to rationally expedite chloride ingress during the experiment, referring to the relationship between surface chloride content and steel corrosion rate derived from the modified Fick's second law [31] and combining conventional concentration parameters of existing accelerated tests, a 5% NaCl solution was selected for this study.

Each freeze-thaw cycle in this test consists of two steps: freezing and thawing, with freezing followed by thawing. The duration of each freeze-thaw cycle should be controlled within 2 to 4 h, and the thawing time should not be less than one quarter of the total freeze-thaw time [32].

2.4 CFRP Sheet Strengthening Scheme

To explore the mechanical performance recovery effect and interface failure mechanism of UHPC with different degrees of damage at an early age after being strengthened with CFRP, this experiment, based on the completion of the freeze-thaw cycle damage test, selected typical UHPC specimens with different degrees of damage for CFRP strengthening research. Three 100 mm × 100 mm × 100 mm cubic specimens were selected for each degree of damage for compressive strengthening tests.

Fig. 4 shows the CFRP strengthening process. This study selects a single-layer circumferential CFRP because it can provide the most effective passive confinement for compression-damaged UHPC, and as the most basic form of reinforcement, it can serve as a benchmark for subsequent research. The construction sequence for strengthening UHPC specimens with CFRP sheets is as follows: Firstly, the surface of the UHPC specimens is sanded smooth with sandpaper (240-grit SiC sandpaper) to remove impurities such as floating slurry and loose layers, ensuring that the bonding surface is clean and smooth. Then, the CFRP sheets are cut and the carbon fiber impregnating adhesive is prepared. A layer of impregnating adhesive with a thickness of 0.2–0.3 mm is applied to ensure even distribution. The main performance indexes of the carbon fiber impregnating adhesive are shown in Table 4. The adhesive is prepared by mixing Component A and Component B at a ratio of 2:1 before use. The cut CFRP sheets are laid on the surface of the specimens that have been coated with carbon fiber impregnating adhesive, and the specimens are wrapped circumferentially in the direction of the fibers. After ensuring that there are no hollows in the wrapped specimens, carbon fiber impregnating adhesive is applied at the lap joints. Subsequently, all specimens pasted with CFRP fabrics were placed in an environment with temperature of 20°C to 25°C and relative humidity of 60% to 80% for three days of curing treatment. Quality control measures involved rolling to expel air and tap testing to verify no hollow debonding. Due to the small thickness of the CFRP sheets, the size difference between the strengthened specimens and the un-strengthened ones can be ignored.



Figure 4: CFRP strengthening process.

Table 4: Performance parameters of the carbon fiber impregnating adhesive.

Performance Items		Performance of A-Component Adhesive	Performance of B-Component Adhesive
Colloidal properties	Tensile strength (MPa)	≥30	≥25
	Tensile elastic modulus (MPa)	≥3500	≥3500
	Elongation (%)	≥1.0	≥1.0
	Flexural strength (MPa)	≥45	≥35
	Compressive strength (MPa)	≥65	≥65
Adhesion ability	Tensile bond strength with concrete (MPa)	≥2.5	≥2.5

2.5 Test Methods

To comprehensively evaluate the performance changes of UHPC specimens after freeze-thaw cycles and CFRP reinforcement, this study systematically analyzed the mass loss, ultrasonic wave velocity, mechanical properties, surface damage and internal microstructure changes of the specimens from macroscopic mechanical properties to microscopic structural characteristics, from surface deterioration to internal damage.

2.5.1 Compressive Strength Test

The loading device is shown in Fig. 5. The maximum load capacity of this universal testing machine is 5000 kN. Compressive strength tests were conducted on cubic UHPC specimens with dimensions of 100 mm × 100 mm × 100 mm. The compressive strength of each specimen was measured at different cycle numbers (0, 30, 60, 90, 120, and 150 times) and after CFRP reinforcement following the cycles. The average value of three parallel samples was adopted for each test result. The compressive strength can be calculated according to Eq. (1).

$$\sigma_C = \frac{P}{I \times b} \tag{1}$$

In the equation: σ_C represents the compressive strength (MPa), P is the failure load (N), I is the length of the specimen's compression surface (mm), b is the width of the specimen's compression surface (mm).

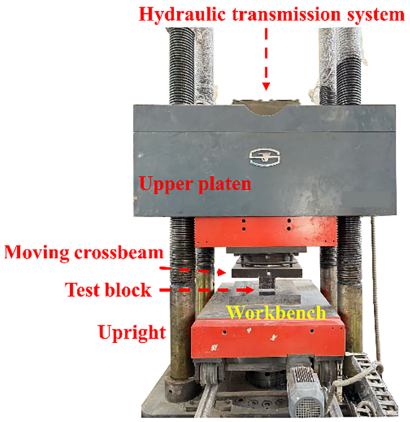


Figure 5: Compressive strength test.

2.5.2 Ultrasonic Testing (UT)

As a typical non-destructive detection technique, ultrasonic velocity testing features simple operation and sensitive response to internal defects and cracks of concrete, which makes it widely used in the characterization of concrete damage [33]. When micro-cracks, increased porosity or accumulated damage occur inside the concrete, the ultrasonic pulse is diffracted at the defect, the propagation path is prolonged, and the wave velocity decreases. According to the theory of elasticity, the wave propagation formula for longitudinal waves within an infinite elastic medium is presented in Eq. (2).

$$v_P = \sqrt{\frac{E\,(1-\mu)}{\rho\,(1+\mu)\,(1-2\mu)}} \tag{2}$$

In the equation: v_p is the propagation velocity of the longitudinal wave in the medium (m/s), E is the elastic modulus (GPa), μ is the Poisson's ratio, ρ is the density (kg/m^3).

As shown in Fig. 6, a dual-port ultrasonic testing system was used to measure the wave velocity in this experiment, with the model being ZBL-U5200 non-metallic ultrasonic detector. The testing equipment included an electrical pulse generator and a pair of sensors (one transmitting sensor and one receiving sensor). Before the ultrasonic testing, calibrate with an acrylic calibration block before each use, and take the average of three stable readings at each measurement point to ensure repeatability. Vaseline was applied as a coupling agent on the surface of the UHPC specimens, the sensor surfaces, and between the receiver and the sensor to reduce the voids at the interfaces and ensure complete contact between the probe and the specimen surface. The average of three replicate samples was adopted for each measured result.

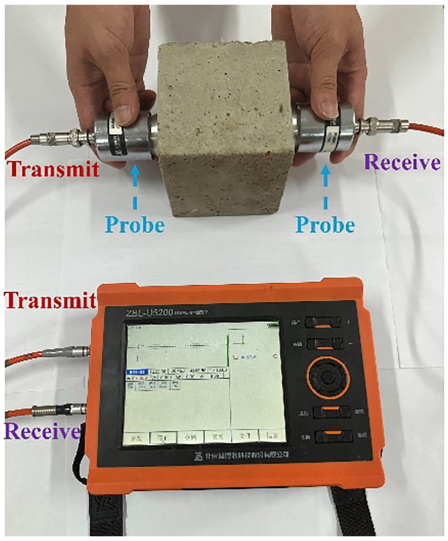


Figure 6: Ultrasonic test.

2.5.3 Quality Loss Test

Mass loss is a direct indicator for evaluating the degree of surface spalling and internal damage of UHPC under freeze-thaw cycles. By measuring the mass change of specimens before and after environmental tests, the degree of material deterioration under environmental loads can be quantitatively reflected, providing basic data for damage evolution analysis. In this experiment, the mass loss rate of early-age UHPC specimens

after different freeze-thaw cycles was tested to assess the degree of surface spalling of UHPC in a freeze-thaw environment, analyze the evolution law of mass loss with the number of cycles, and provide a basis for the subsequent correlation analysis of macroscopic performance degradation and microscopic structure evolution.

The mass loss rate is calculated according to Eq. (3). For each set of UHPC specimens, the mass loss ratio was tested at an interval of 30 freeze-thaw cycles. The average value of three test samples is taken for each test result.

$$\Delta W_{\mathrm{n}} = \frac{M_0 - M_{\mathrm{n}}}{M_0} \times 100\% \tag{3}$$

In the equation: ΔW_{n} represents the mass loss rate (%) after the nth cycle, M_0 is the initial mass of the specimen (g), and M_{n} is the mass of the specimen (g) after the nth cycle.

2.5.4 Performance Testing of CFRP Reinforcement

To explore the mechanical property recovery effect and interface failure mechanism of UHPC with different degrees of damage at an early age after CFRP reinforcement, typical UHPC specimens with different damage degrees were selected for CFRP reinforcement research after every 30 freeze-thaw cycles. Three 100 mm × 100 mm × 100 mm cubic specimens were selected for each damage degree to conduct the CFRP-reinforced compressive strength test. Fig. 7 shows the flowchart of CFRP-reinforced damaged UHPC specimens and compressive strength test.



Figure 7: CFRP strengthening test procedure.

To quantitatively evaluate the strengthening effect of CFRP, the strength recovery rate η is introduced, as shown in Eq. (4). This indicator reflects the degree of strength recovery of the specimen after CFRP strengthening relative to the intact UHPC.

$$\eta = \frac{f_{c,g}}{f_{c,0}} \times 100\% \tag{4}$$

In the equation: η represents the strength recovery rate (%), $f_{c,g}$ is the compressive strength (MPa) of the specimen after undamaged and strengthened, and $f_{c,0}$ is the compressive strength (MPa) of the undamaged and unstrengthened specimen.

In addition, the strengthening efficiency coefficient α is introduced as shown in Eq. (5). This indicator reflects the direct improvement effect of CFRP strengthening on the damaged specimens, excluding the influence of the damage itself.

$$\alpha = \frac{f_{c,k}}{f_{c,u}} \times 100\% \tag{5}$$

In the equation: α represents the reinforcement coefficient (%), $f_{c,k}$ is the compressive strength (MPa) of the specimen after damage and reinforcement, and $f_{c,u}$ is the compressive strength (MPa) of the specimen after damage but without reinforcement.

2.5.5 Microstructure

The microstructural characteristics of UHPC after various freeze-thaw cycles were investigated via scanning electron microscopy (SEM), while energy dispersive X-ray spectroscopy (EDS) was adopted to determine the elemental composition and relative content. The preparation quality of SEM-EDS specimens directly affects the imaging effect and the reliability of the analysis results. Specimens subjected to different numbers of freeze-thaw cycles are selected, and after breaking, block samples of approximately 10 mm × 10 mm × 10 mm are cut from the central area of the specimen. When sampling, the edges of the specimen should be avoided to prevent additional damage during the cutting process. For specimens that require observation of the erosion interface, samples should be taken from the surface of the specimen toward the interior (0–5 mm from the surface).

3 Test Results

3.1 Compressive Strength Analysis

Fig. 8 shows the compressive strength of early-age UHPC at 0, 30, 60, 90, 120, and 150 freeze-thaw cycles and the corresponding days of curing, as well as the compressive strength after CFRP reinforcement. The initial compressive strength (cured for 7 d but without cycles) was 80.1 MPa. Since this group did not undergo freeze-thaw cycles, the strength was only affected by the curing age and showed a continuous upward trend with the increase of age. It rose to 83.4 MPa at 30 cycles, 87.5 MPa at 60 cycles, 91.6 MPa at 90 cycles, increased to 95.7 MPa at 120 cycles, and further rose to 99.8 MPa at 150 cycles. At the curing days corresponding to 150 freeze-thaw cycles, the strength increased by 24.6% compared to the initial strength.

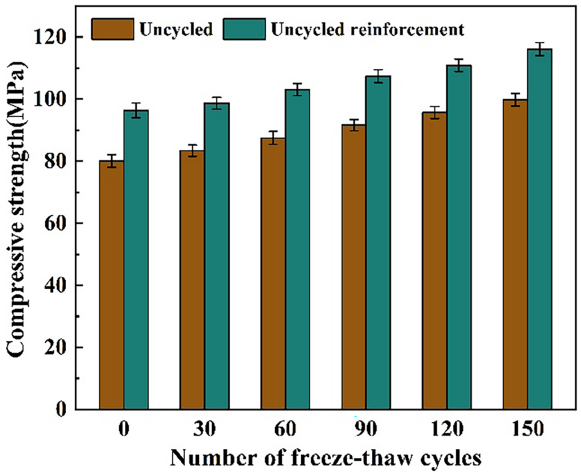


Figure 8: Compressive strength of unfrozen and unreinforced specimens. Error bars represent standard deviation (n = 3).

For specimens that were not subjected to freeze-thaw cycles but were reinforced with CFRP, the compressive strength remained at the highest level throughout. The strength was 96.4 MPa at 0 cycles (after 7 d of curing and CFRP reinforcement), rose to 98.7 MPa at 30 cycles, reached 103.1 MPa at 60 cycles, 107.4 MPa at 90 cycles, and reached 110.9 MPa at 120 cycles, further increasing to 116.1 MPa at 150 cycles. Compared with the non-cycled and non-reinforced group, the strength increase at each age was 15.2% to 16.8 MPa. It can be seen that CFRP reinforcement can effectively enhance the mechanical properties of intact specimens.

Fig. 9 shows the compressive strength of early-age UHPC after freeze-thaw cycles and reinforced with CFRP. It can be seen from the figure that the compressive strength shows a continuous downward trend with the increase of freeze-thaw cycles. After 30 cycles, it drops to 76.7 MPa (a decrease of 4.2%), after 60 cycles to 73.6 MPa (a decrease of 8.1%), after 90 cycles to 70.4 MPa (a decrease of 12.1%), after 120 cycles to 67.1 MPa (a decrease of 16.2%), and after 150 cycles to only 64.2 MPa (a decrease of 19.9%). In this test, due to the synergistic effect of chloride salts and freeze-thaw, the deterioration in the salt-frost environment is more significant, and the damage is relatively large. Compared with the specimens after freeze-thaw cycles, CFRP reinforcement significantly improves the compressive strength at each cycle. The strength is 91.3 MPa at 0 freeze-thaw cycles, 89.5 MPa after 30 cycles, 85.1 MPa after 60 cycles, 81.2 MPa after 90 cycles, 76.8 MPa after 120 cycles, and 72.6 MPa after 150 cycles. The strengthening mechanism of CFRP reinforcement for freeze-thaw damaged UHPC mainly includes: first, providing lateral confinement. The CFRP sheet wraps the specimen to form circumferential confinement, restricting the lateral expansion of the freeze-thaw damaged specimen under axial load and inhibiting the propagation and coalescence of micro-cracks. Second, load sharing. The CFRP sheet forms an efficient bond with the UHPC surface, which can share part of the axial load and enhance the overall load-bearing capacity of the specimen [34]. Notably, at the damage level after 30 cycles, the strength increases by 16.69%, and at the damage level after 150 cycles, the strength increases by 13.08%. This indicates that CFRP reinforcement has a good repair effect on early freeze-thaw damage, but when the damage accumulates to a certain extent, the reinforcement effect will be constrained.

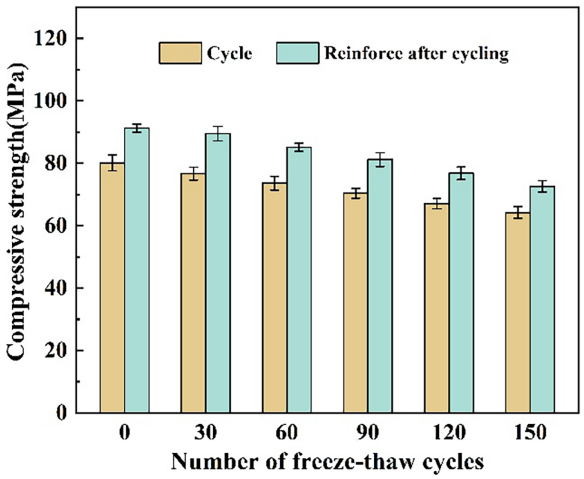
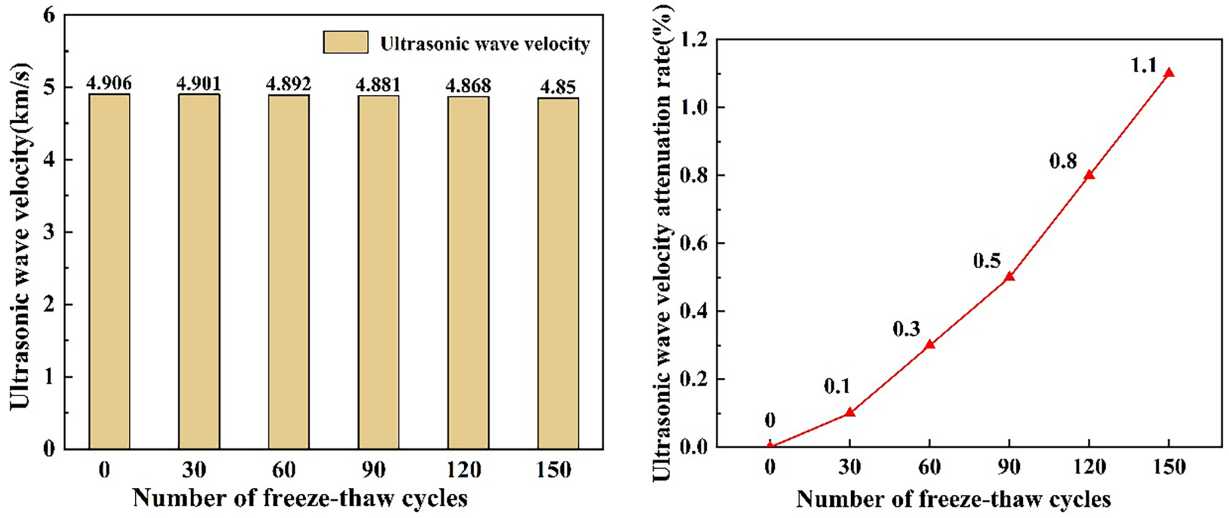


Figure 9: Compressive strength of reinforced specimens after freeze-thaw cycles. Error bars represent standard deviation (n = 3).

3.2 Ultrasonic Wave Velocity Analysis

Fig. 10 shows the ultrasonic wave velocity and its changing trend of UHPC specimens under freeze-thaw cycles. Among them, (a) is ultrasonic wave velocity, (b) is wave velocity attenuation rate. Under the

initial condition of 0 freeze-thaw cycle, the ultrasonic wave velocity of the sample reached 4.906 km/s. After 30 cycles of freeze-thaw action, the velocity dropped to 4.901 km/s, representing a decline of merely 0.10%. After 60 cycles, it was 4.892 km/s; after 90 cycles, it was 4.881 km/s; and after 120 cycles, it was 4.868 km/s. When the number of cycles reached 150, the wave velocity further decreased to 4.850 km/s, with a cumulative decrease of 0.056 km/s compared to the initial state, and a total decrease of 1.14%. Overall, the decrease in wave velocity gradually expanded with the increase in the number of cycles, showing a clear cumulative damage effect.



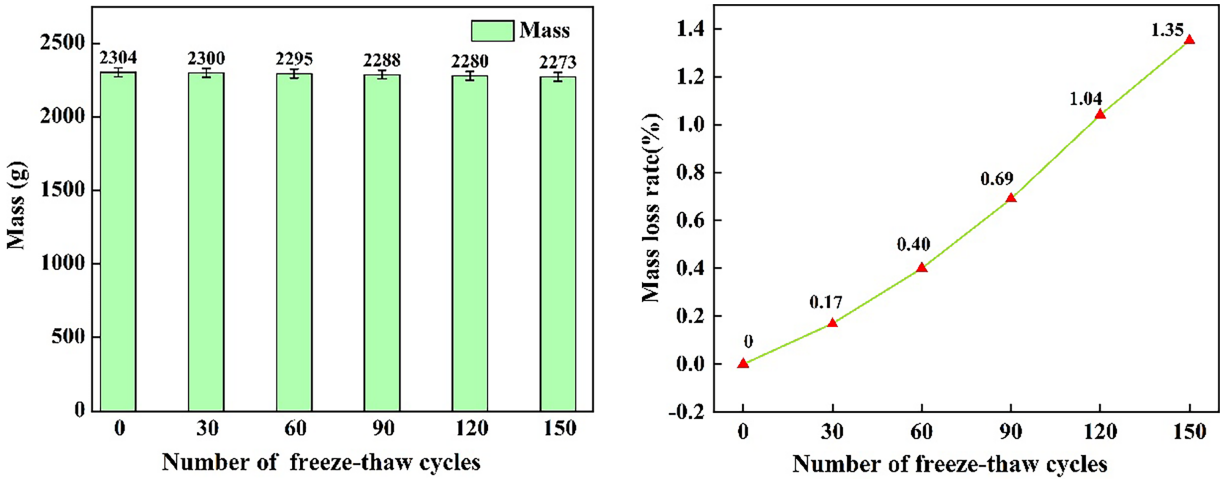
(**a**) Ultrasonic wave velocity (**b**) Wave velocity attenuation rate

Figure 10: Ultrasonic wave velocity and its changing trend.

Early-age UHPC shows a relatively slow trend of wave velocity attenuation under freeze-thaw cycles, maintaining a high wave velocity of 4.850 km/s after 150 cycles, demonstrating its excellent resistance to freeze-thaw. This is due to its extremely low porosity, dense microstructure, and the bridging restraint effect of copper-plated steel fibers, which is consistent with Shah et al. [35] findings on the durability performance of steel fiber UHPC at low temperatures. However, the continuous decline in wave velocity also indicates that early-age UHPC is not completely immune to freeze-thaw damage, especially with the damage intensifying after 120 freeze-thaw cycles, and the damage effect will further accumulate, ultimately resulting in the attenuation of mechanical and durability properties.

3.3 Mass Loss Analysis

Fig. 11 shows the variation trend of the mass and loss rate of UHPC specimens at an early age after different freeze-thaw cycles. Among them, (a) is post-cycle mass, (b) is trend of change in quality loss rate. As illustrated in the figure, the mass loss rate of UHPC specimens increases gradually as the number of freeze-thaw cycles rises, and the increasing amplitude is far smaller than that of conventional concrete. After 30 freeze-thaw cycles, the mass loss rate is only 0.17%, increasing to 0.40% after 60 cycles, 0.69% after 90 cycles, 1.04% after 120 cycles, and 1.35% after 150 cycles. All tested samples exhibit mass loss rates considerably lower than the 5% limit specified in relevant freeze-thaw specifications. Previous research by Lyu et al. [36] reported that the mass loss of all groups remained below 1.53% even after 300 salt freeze-thaw cycles. In the present study, the mass loss rate was 1.35% after 150 cycles, showing good agreement with the published findings.



(**a**) Post-cycle mass (**b**) Trend of change in mass loss rate

Figure 11: Mass and change trend after cycling.

3.4 Analysis of Specimen Surface Damage

Fig. 12 shows the surface damage morphology of UHPC specimens under freeze-thaw cycles. It can be seen from the figure that after 30 cycles, the specimens have only a few original pores, no obvious spalling, and extremely low mass loss. After 60 cycles, local pores of the specimens expand, and a small amount of matrix debris falls off due to freeze-thaw expansion, with a slow mass loss rate. After 90 cycles, microcracks appear, fibers are exposed, and the matrix at the crack tips breaks and falls off, with an accelerated mass loss rate. After 120 cycles, cracks connect and local spalling occurs, and the mass loss reaches a relatively high level. After 150 cycles, the surface becomes rough, a large number of fibers are exposed, the matrix falls off, and the mass loss further increases. At the same time, it can be seen from the figure that after 30, 60, 90, 120, and 150 freeze-thaw cycles, the surface of the specimen shows significant damage areas of approximately 2%, 10%, 30%, 50%, and 80%, respectively.

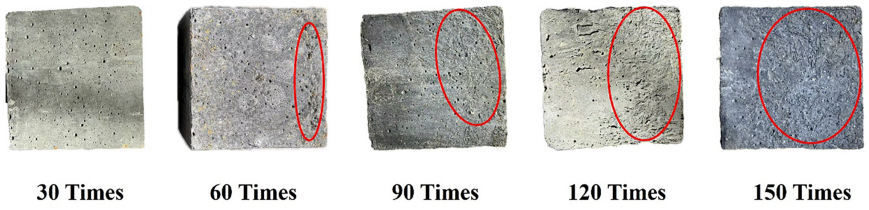


Figure 12: Surface morphology of specimens after different cycle numbers.

3.5 Analysis of CFRP Strengthening Performance

Fig. 13 shows typical images of damaged UHPC specimens reinforced with CFRP after cyclic loading and compressive strength testing (the tilt of the specimens in the images is not due to improper placement causing eccentric failure, but is due to the angle at which the photos were taken on site). From the figure, it can be seen that CFRP-reinforced UHPC specimens exhibit three typical failure modes after the compressive strength test, corresponding to matrix cohesion failure, interface delamination failure, and mixed failure modes.

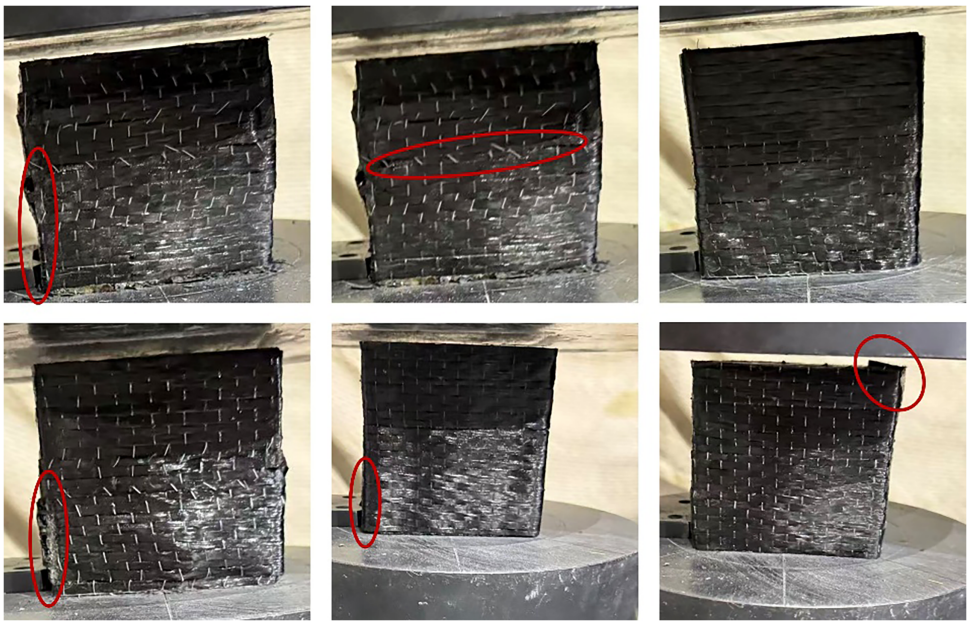


Figure 13: Damage pattern of the specimen's compressive strength after reinforcement.

In this test, η showed a downward trend. The fundamental reason is that the growth rate of the strength after reinforcement is lower than the natural growth rate of the strength of the unreinforced specimen. Under standard curing conditions, the strength of UHPC increases continuously with age, as cement continues to hydrate to form C-S-H gel, and the hydration products continuously fill the pores, leading to densification of the matrix. Although the strength of the reinforced specimens also increases with age, there is a key difference: the CFRP sheets were adhered at different ages, resulting in different interface bonding states. As the curing time increases, the matrix of the specimens gradually densifies, making it increasingly difficult for the CFRP adhesive to penetrate, thus reducing the reinforcement effect and causing η to gradually decrease.

Fig. 14 shows the trend of α after freeze-thaw cycles. As shown in the figure, the value of α gradually declines as the number of freeze-thaw cycles increases. At 0 cycles, α is 116.7%, at 30 cycles, α is 116.0%, at 60 cycles, α is 115.6%, at 90 cycles, α is 115.3%, at 120 cycles, α is 114.5%, and at 150 cycles, α is 113.1%. CFRP maintains efficient reinforcement capability even under severe freeze-thaw damage, and after 150 cycles, it can still restore the strength to more than 113% of the damaged specimen. But α is also continuously decreasing, hydrostatic pressure serves as the dominant factor causing UHPC damage under freeze-thaw cycles, which results in serious ITZ debonding, microcrack initiation and growth, as well as the structural deterioration of C-S-H hydration products. These microscopic damages directly affect the strengthening effect of CFRP. Freeze-thaw damage will weaken the strengthening efficiency of CFRP. The more severe the damage, the smaller the increase in the strength of CFRP.

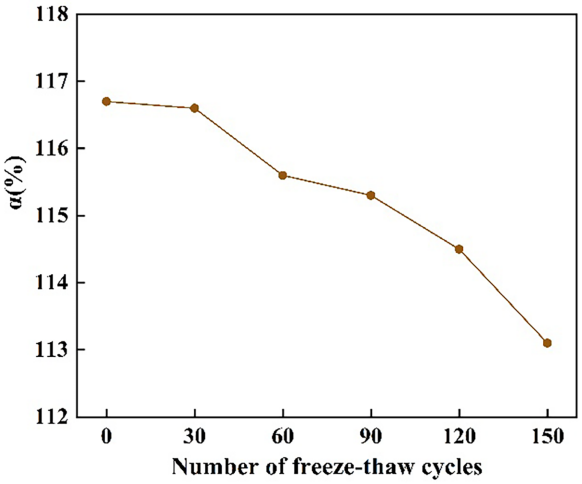
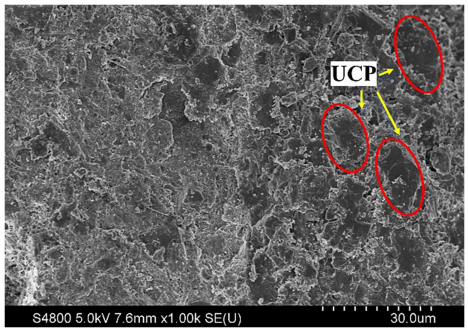


Figure 14: Trend of α changes after freeze-thaw cycles.

3.6 Microstructure Evolution (SEM-EDS) Analysis

With reference to SEM observations, the microstructural features of early-age UHPC subjected to various freeze-thaw cycles were systematically characterized. By analyzing the development degree of hydration products in the matrix, the bonding state of ITZ, the pore characteristics, and the initiation and propagation laws of voids and microcracks, the internal damage evolution mechanism of the material under the action of freeze-thaw cycles was revealed.

Fig. 15 shows the SEM images of UHPC specimens after different freeze-thaw cycles. Among them, (a) is 30 freeze-thaw cycles, (b) is 60 freeze-thaw cycles, (c) is 90 freeze-thaw cycles, (d) is 120 freeze-thaw cycles, and (e) is 150 freeze-thaw cycles. It can be seen from the figure that the microstructure integrity and density of the specimens are the best after 30 freeze-thaw cycles, presenting a continuous, uniform and dense microstructure overall, without obvious loose structural areas. The surfaces of aggregates and unhydrated particles (UCP) are fully covered by hydration products, and the ITZ is dense and continuous, without obvious debonding or crack development. This indicates that the interfacial bonding performance is good and the microstructure still maintains a high degree of integrity.



(**a**) 30

Figure 15: (Continued)

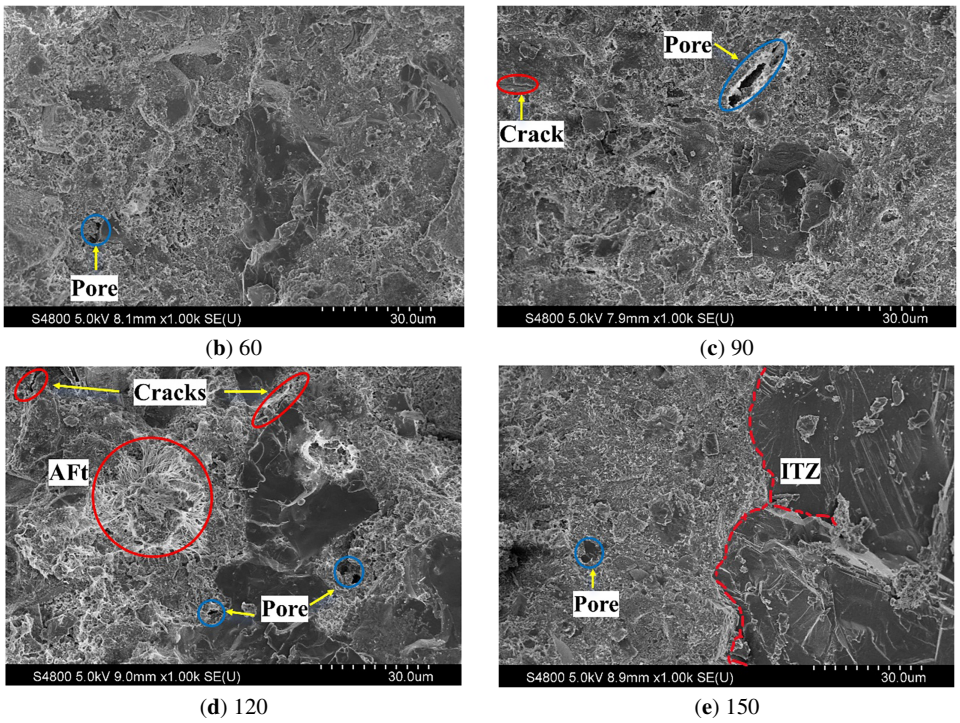


Figure 15: SEM images after different freeze-thaw cycles.

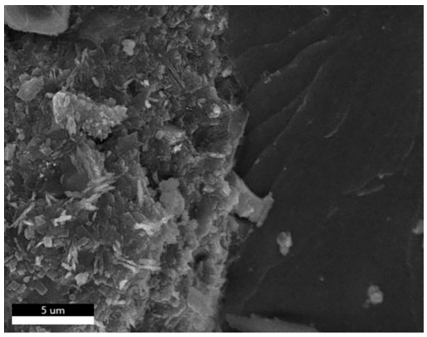
After 60 freeze-thaw cycles, the microstructure of the specimens remained relatively dense as a whole, but compared with the specimens after 30 cycles, slight freeze-thaw damage characteristics had emerged. The matrix calcium silicate hydrate (C-S-H) gel maintained a continuous and interwoven state overall, but the packing density of the gel in some local areas slightly decreased, and the structural uniformity was somewhat reduced. ITZ began to show weak signs of deterioration, with a slight increase in the number of pores, which were still mainly isolated micro-pores, and no obvious through channels were observed. A few short and fine cracks were visible in some local areas, with both the length and width of the cracks being small, and most of them terminated within the matrix without showing an expanding and penetrating trend.

After 90 freeze-thaw cycles, the degree of deterioration of the microstructure of the specimens further intensified, showing the characteristics of freeze-thaw damage development. However, the microstructure still maintained relatively good integrity. The density of the C-S-H gel in the matrix decreased, and loose gel structure and uneven accumulation occurred in some areas. The bonding strength between the hydration products decreased. At the same time, micro-cracks and pores appeared, and the cracks showed an extending and expanding trend, and began to show signs of local connectivity.

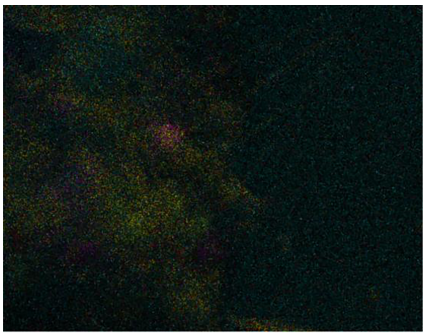
Upon 120 freeze-thaw cycles, serious freeze-thaw deterioration occurred in the internal microstructure of the sample, accompanied by a notable decline in matrix integrity. The C-S-H gel structure of the matrix shows a fragmented and loose state, and the continuous skeleton has been damaged. At the same time, a large number of microcracks have emerged, forming a network of penetrating cracks, which disrupts the continuity of the matrix. The number and size of pores have significantly increased, and a large number of pores are interconnected to form permeation channels, providing convenient paths for the transmission of water and eroding ions. The deterioration of the microstructure has developed from local defects to overall structural damage, this inevitably results in the decline of macroscopic mechanical performance and durability, while exacerbating the development of internal damage.

After 150 freeze-thaw cycles, the microstructure of the specimens was most significantly damaged, and the degree of freeze-thaw damage was the most severe. The C-S-H gel structure of the matrix was nearly disintegrated, presenting a highly loose and fragmented debris-like morphology. The skeleton of the hydration products basically lost its load-bearing and constraining capacity. The ITZ failed, and wide and penetrating cracks appeared between the aggregates and the hydrated matrix. The interfacial bonding was severely damaged, and the internal structure presented a discontinuous state.

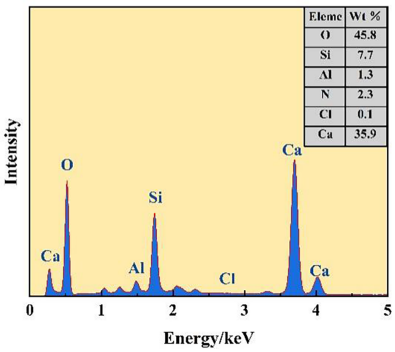
SEM-EDS can qualitatively and quantitatively analyze the elemental composition of micro-regions, assisting in the identification of the types and distributions of erosion products. Figs. 16–20 are the EDS images after 30, 60, 90, 120 and 150 freeze-thaw cycles respectively. Among them, (a) is scanning area, (b) is EDS mapping and (c) is EDS energy spectrum.



(**a**) Scanning area

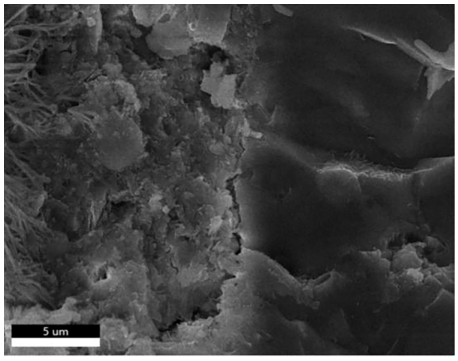


(**b**) EDS mapping



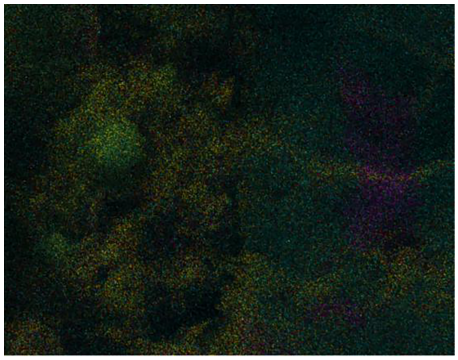
(**c**) EDS energy spectrum

Figure 16: EDS image after 30 freeze-thaw cycles.

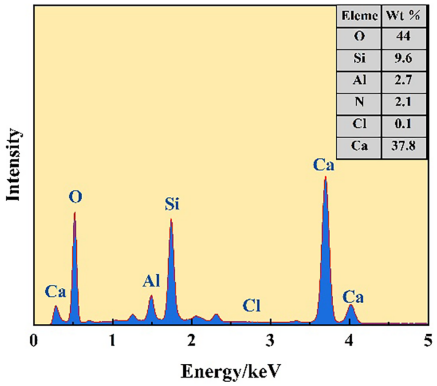


(**a**) Scanning area

Figure 17: (Continued)

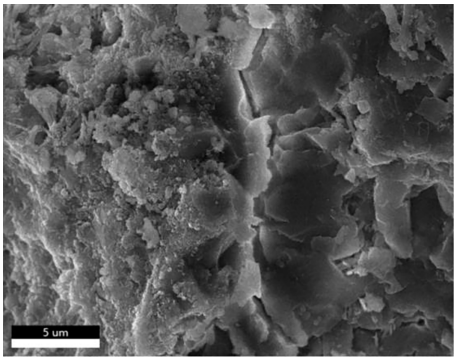


(**b**) EDS mapping

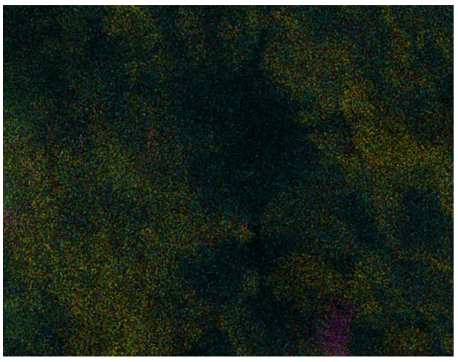


(**c**) EDS energy spectrum

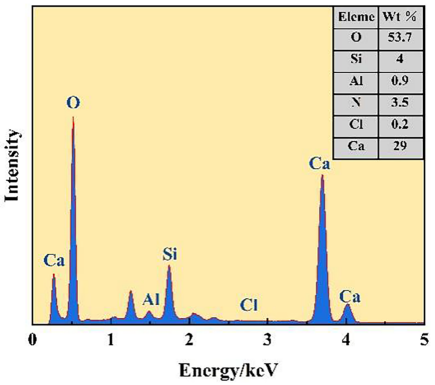
Figure 17: EDS image after 60 freeze-thaw cycles.



(**a**) Scanning area

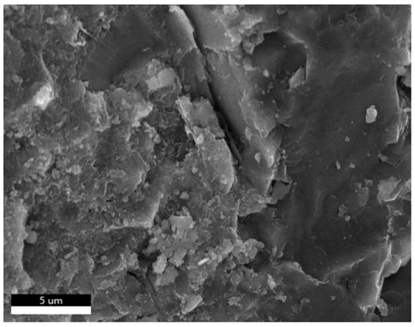


(**b**) EDS mapping

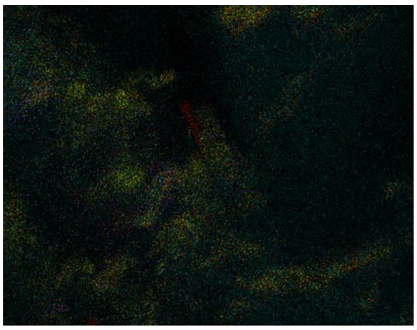


(**c**) EDS energy spectrum

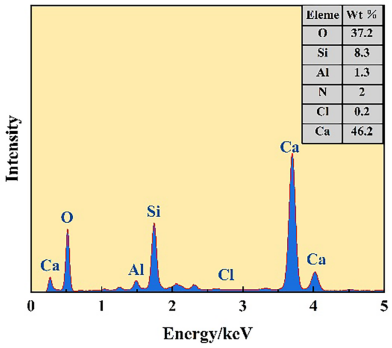
Figure 18: EDS image after 90 freeze-thaw cycles.



(**a**) Scanning area

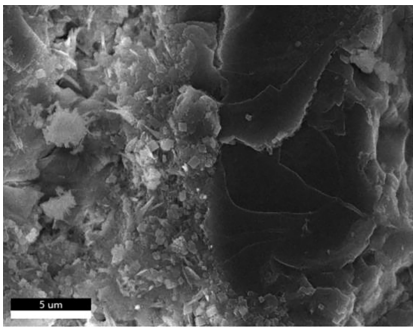


(**b**) EDS mapping

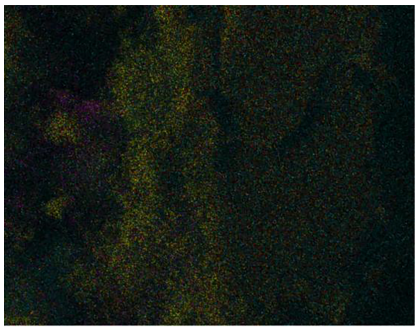


(**c**) EDS energy spectrum

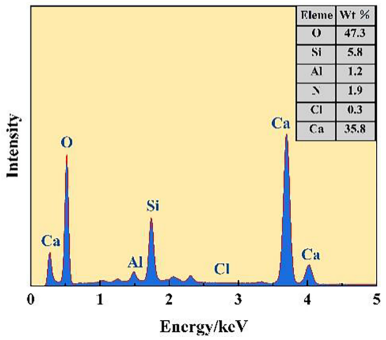
Figure 19: EDS image after 120 freeze-thaw cycles.



(**a**) Scanning area



(**b**) EDS mapping



(**c**) EDS energy spectrum

Figure 20: EDS image after 150 freeze-thaw cycles.

EDS analysis at different freeze-thaw cycles indicates that the surface chloride ion mass fraction of UHPC presents an increasing trend with the rising number of freeze-thaw cycles. After 30 and 60 freeze-thaw cycles, the mass fraction of chloride ions on the surface of the specimens is both 0.1%, indicating that chloride ions have begun to penetrate into the surface pores through capillary adsorption in the early stage of freeze-thaw. After 90 and 120 freeze-thaw cycles, the mass fraction of chloride ions rises to 0.2%. Repeated freezing and thawing of pore water during freeze-thaw cycling accelerates the migration of chloride ions into the UHPC interior. Following 150 freeze-thaw cycles, the chloride ion mass fraction rises further to 0.3%. Zhong et al. [13] studied microcracked UHPC under freeze-thaw cycles in a 4% NaCl solution and found that even after 300 freeze-thaw cycles, the chloride ion concentration in UHPC remained at a relatively low level (generally below 0.5%). Fig. 21 illustrates the change law of chloride ion mass fraction. It is worth noting that the SEM-EDS in this experiment has certain limitations, and it is recommended that future studies use multi-point area scans to obtain more reliable quantitative analysis results.

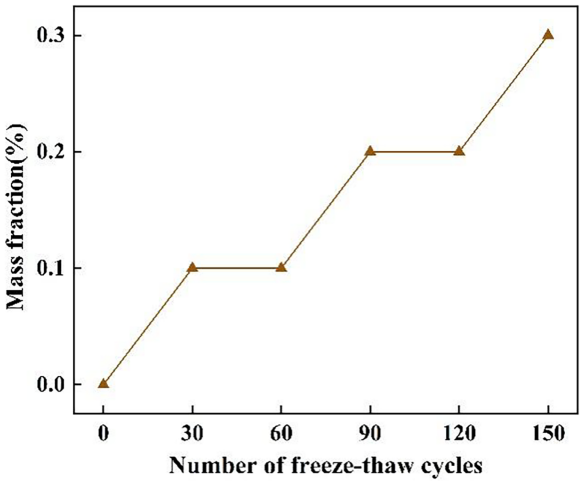


Figure 21: Changes in the mass fraction of chloride ions.

Fig. 22 shows the compressive strength and the variation trend of the Ca/Si atomic ratio after freeze-thaw cycles, since the test differences are not significant, only a qualitative trend is indicated. It can be seen from the figure that both the compressive strength of the specimens and the Ca/Si ratio of the matrix decrease with the increase of the number of freeze-thaw cycles. This phenomenon is mainly attributed to the following aspects. Firstly, calcium ion leaching: during freeze-thaw cycles, the repeated freezing and thawing of pore water promotes the dissolution and migration of calcium ions, resulting in a decrease in the Ca/Si ratio of C-S-H gel. Secondly, secondary hydration of silica fume: UHPC contains a large amount of silica fume, and its pozzolanic reaction continuously consumes calcium hydroxide to form C-S-H gel with a low Ca/Si ratio. The wetting stage during freeze-thaw cycles provides water for secondary hydration, promoting the reaction. Finally, the effect of chloride salt erosion: chloride ions react with calcium sulfoaluminate (AFm) phase to form Friedel's salt, consuming some calcium ions and thus altering the elemental distribution.

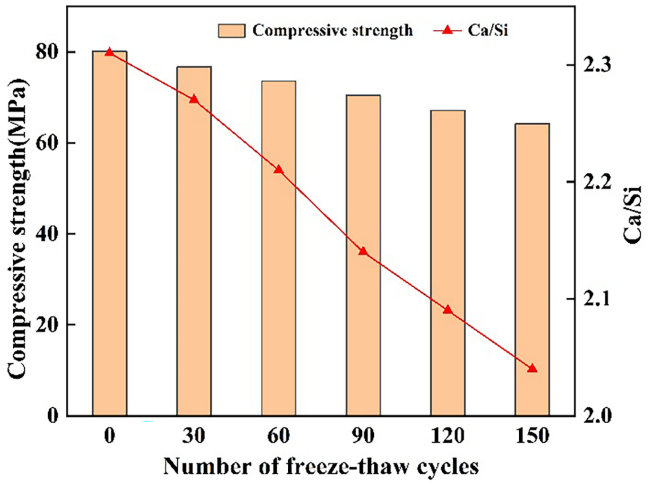


Figure 22: Strength after freeze-thaw and Ca/Si atomic ratio.

4 Conclusion

Based on the early-age (only 7 d of curing) freeze-thaw cycle—chloride salt erosion coupling test, combined with multiple analysis techniques, this paper systematically studies the strength improvement effect and mechanism of CFRP reinforcement on early-age freeze-thaw damaged UHPC, the present work is intended to clarify the failure evolution characteristics of UHPC subjected to freeze-thaw cycling and the mechanical behavior of CFRP strengthening. According to the experimental and analytical results, the conclusions can be summarized as follows:

(1) Early-age freeze-thaw cycles induce progressive deterioration of UHPC, characterized by increased mass loss, reduced ultrasonic velocity, and decreased compressive strength. Microscopic analysis reveals that chloride penetration, steel fiber corrosion, and increased porosity are the primary damage mechanisms.

(2) CFRP circumferential strengthening effectively restores the compressive strength of freeze-thaw damaged UHPC, with the reinforcement efficiency coefficient α remaining above 100% after 150 cycles. However, strengthening efficiency declines with increasing cycle numbers due to more severe hydrostatic pressure-induced damage.

(3) The Ca/Si atomic ratio decreases under freeze-thaw-chloride coupling, resulting from calcium ion leaching and secondary hydration of silica fume, which accelerates matrix decalcification and microstructural deterioration.

(4) This study validates CFRP as a viable post-damage reinforcement for early-age UHPC in cold regions and establishes a dual evaluation system (η and α) for quantitative assessment. Future work should explore longer curing times and complex coupling conditions.

(5) Engineering application recommendation: the reinforcement effect is best when the strength loss is 15%–20%. If the loss is less than 15%, reinforcement is not necessary (natural curing can compensate); if it is 15%–20%, reinforcement is recommended ($\alpha > 113\%$); if the loss is greater than 20%, surface repair should be combined. A conservative recommendation is to use 15% strength loss as the trigger value for reinforcement.

Acknowledgement: Not applicable.

Funding Statement: The writers gratefully acknowledge the financial support of the National Natural Science Fund of China (52168072, 51808467, https://www.nsfc.gov.cn/, awarded to Dewen Liu), Scientific Research Fund Project of the Yunnan Provincial Department of Education (2025J0644, https://jyt.yn.gov.cn/article/, 2147452221, awarded to Qian Wang).

Author Contributions: Conceptualization, Yongbing Sun; Experimental design, Yongbing Sun; Feasibility analysis, Qian Wang and Yuexia Yang; Data collection and organization, Yongbing Sun and Canhuan Pan; Writing and original draft preparation, Yongbing Sun; Writing and review and editing, Dewen Liu; Supervision, Dewen Liu. All authors reviewed and approved the final version of the manuscript.

Availability of Data and Materials: Data available on request from the authors.

Ethics Approval: Not applicable.

Conflicts of Interest: The authors declare no conflicts of interest.

References

1. Du J, Meng W, Khayat KH, Bao Y, Guo P, Lyu Z, et al. New development of ultra-high-performance concrete (UHPC). Compos Part B Eng. 2021;224(9):109220. doi:10.1016/j.compositesb.2021.109220.
2. Akeed MH, Qaidi S, Ahmed HU, Faraj RH, Mohammed AS, Emad W, et al. Ultra-high-performance fiber-reinforced concrete. Part I: developments, principles, raw materials. Case Stud Constr Mater. 2022;17(5):e01290. doi:10.1016/j.cscm.2022.e01290.
3. Li J, Wu Z, Shi C, Yuan Q, Zhang Z. Durability of ultra-high performance concrete—a review. Constr Build Mater. 2020;255(8):119296. doi:10.1016/j.conbuildmat.2020.119296.
4. Swenty MK, Graybeal BA. Characterization of materials used in field-cast precast concrete connections. PCI J. 2017;62(6):33–44. doi:10.15554/pcij62.6-03.
5. Wan L, Wendner R, Liang B, Cusatis G. Analysis of the behavior of ultra high performance concrete at early age. Cem Concr Compos. 2016;74(31):120–35. doi:10.1016/j.cemconcomp.2016.08.005.
6. Hasnat A, Ghafoori N. Freeze-thaw resistance of nonproprietary ultrahigh-performance concrete. J Cold Reg Eng. 2021;35(3):04021008. doi:10.1061/(ASCE)CR.1943-5495.0000255.
7. Liu J, Ye H, Yu K, Li H, Gan Z, Wang Y, et al. Study on the influence of freeze-thaw cycles on the shear performance of the UHPC-NC interface with planted reinforcement. Buildings. 2025;15(22):4068. doi:10.3390/buildings15224068.
8. Chi K, Li J, Shao R, Wu C. Experimental study on dynamic characterisation of ultra-high performance concrete (UHPC) after cryogenic freeze-thaw cycles. Cem Concr Compos. 2025;160(5):106011. doi:10.1016/j.cemconcomp.2025.106011.
9. Liu K, Li J, Wu T, Xie T, Sang Y, Lin Y, et al. Interfacial bond performance and degradation mechanisms of UHPC-normal concrete composites in aggressive environments. Structures. 2026;85(4):111152. doi:10.1016/j.istruc.2026.111152.
10. Hao L, Liu Y, Xiao J. Durability of recycled aggregate thermal insulation concrete under combined flexural loading and freeze-thaw cycles. Constr Build Mater. 2021;272(2):121652. doi:10.1016/j.conbuildmat.2020.121652.
11. Mészöly T, Ofner S, Randl N. Effect of combining fiber and textile reinforcement on the flexural behavior of UHPC plates. Adv Mater Sci Eng. 2020;2020(1):9891619. doi:10.1155/2020/9891619.
12. Peng G, Gao Y, Tarantino AM, Wang A, Kang S, Hu C, et al. Durability enhancement of ultra-high-performance concrete repair materials under chloride, sulfate, and freeze-thaw conditions through synergistic effects of silica fume, nucleating agents, and fibers. Constr Build Mater. 2025;504:144606. doi:10.1016/j.conbuildmat.2025.144606.

13. Zhong R, Ai X, Pan M, Yao Y, Cheng Z, Peng X, et al. Durability of micro-cracked UHPC subjected to coupled freeze-thaw and chloride salt attacks. Cem Concr Compos. 2024;148:105471. doi:10.1016/j.cemconcomp.2024.105471.
14. Weng Y, Qiao P, Sun L. Effect of microstructural damage evolution on tensile strength of ultra-high performance concrete: a multiscale numerical scheme. Int J Damage Mech. 2025;34(6):1014–33. doi:10.1177/10567895251329950.
15. Banik D, Yadak O, Floyd R. Flexural performance of pre-cracked UHPC with varying fiber contents and fiber types exposed to freeze-thaw cycles. J Compos Sci. 2026;10(1):5. doi:10.3390/jcs10010005.
16. Zheng H, Zhang W, Li B, Zhu J, Wang C, Song G, et al. Recent advances of interphases in carbon fiber-reinforced polymer composites: a review. Compos Part B Eng. 2022;233(2):109639. doi:10.1016/j.compositesb.2022.109639.
17. Kishi N, Kawarai T, Komuro M. Assessment of the static and impact resistance behavior of flexurally strengthened RC beams by bonding medium-elasticity CFRP sheets. Int J Prot Struct. 2026;17(2):714–28. doi:10.1177/20414196251391441.
18. Alotaibi NK, Shekarchi WA. Influence of geometric parameters on bent CFRP and GFRP spike anchors: experimental investigation and design recommendations. Eng Struct. 2026;360(1):122808. doi:10.1016/j.engstruct.2026.122808.
19. Jiang Z, Zhu Z, Friedrich LF, Cezar ES, Chen J, Lacidogna G, et al. Multi-technical analysis of damage process in GFRP-bar reinforced concrete beam. Eng Struct. 2026;348(2):121803. doi:10.1016/j.engstruct.2025.121803.
20. Peng S, Min TR, Peng S, Xie XQ, Yao YK, Jia YS. Compression behavior of CFRP-confined recycled aggregate concrete under combined effects of sulfate corrosion and freeze-thaw cycles. Constr Build Mater. 2025;473(17):141064. doi:10.1016/j.conbuildmat.2025.141064.
21. Feng Z, Wu J, Hu D, Zhao L. Axial compression performance of CFRP confined concrete columns with various types of recycled coarse aggregate under freeze-thaw action. Structures. 2025;81(5):110232. doi:10.1016/j.istruc.2025.110232.
22. Zhang K, Wu Q, Liu B, Zhao Y, Yu Y, Yang R. Enhancement and mechanisms of interfacial bonding performance in CFRP reinforced wind-sand eroded concrete. Compos Part B Eng. 2026;316(4):113548. doi:10.1016/j.compositesb.2026.113548.
23. Wang Q, Guo S, Chen G, Lu C. Axial compressive behavior and stress-strain model of CFRP-UHPC composite-strengthened concrete columns. J Build Eng. 2026;120(12):115501. doi:10.1016/j.jobe.2026.115501.
24. Che J, Liu C, Wu P, Li X, Liu H, Doh SI. Comparative study on seismic behavior of corroded RC columns strengthened by ECC combined with steel cage/fiber grid/CFRP. Structures. 2024;66:106866. doi:10.1016/j.istruc.2024.106866.
25. Xu YY, Huang JQ. Cyclic performance of corroded reinforced concrete short columns strengthened using carbon fiber-reinforced polymer. Constr Build Mater. 2020;247(9):118548. doi:10.1016/j.conbuildmat.2020.118548.
26. Jiang Z, Zhu Z, Lacidogna G, Chen J, Li B. Experimental validation and fracture mechanics analysis of an innovative UHPC-based material for structural strengthening. Mech Res Commun. 2026;151(6):104603. doi:10.1016/j.mechrescom.2025.104603.
27. Sitnikov I, Sitnikov V. Early structure formation in concrete with water-to-cement ratio 0.2. Farmington Hills, MI, USA: American Concrete Institute, ACI Special Publication; 2018.
28. ASTM C1856/C1856M-24. Standard practice for fabricating and testing specimens of ultra-high performance concrete. West Conshohocken, PA, USA: ASTM; 2017.
29. Lian X, Liu X, Lyu X, Yang Q, Chen J, Yu X, et al. Research on the conductivity and self-sensing properties of high strength cement-based material with oriented copper-coated steel fibers. J Build Eng. 2024;86(5):108845. doi:10.1016/j.jobe.2024.108845.
30. Gao YH, Zhang JZ, Zhang S, Zhang YR. Probability distribution of convection zone depth of chloride in concrete in a marine tidal environment. Constr Build Mater. 2017;140(2):485–95. doi:10.1016/j.conbuildmat.2017.02.134.
31. Tavares F, Andrade C. Analytical solution of second Fick's law for chlorides considering accumulation at the bar surface. J Build Eng. 2026;125(3):116005. doi:10.1016/j.jobe.2026.116005.
32. GB/T 50082-2024. Standard for test methods of long-term performance and durability of concrete. Beijing, China: National Standardization Administration; 2024.

33. Wang Y, Mukherjee A, Castel A. Ultrasonic guided waves for monitoring incipient corrosion in reinforced concrete with top-bar defect. Cem Concr Compos. 2023;141(6):105116. doi:10.1016/j.cemconcomp.2023.105116.
34. Monti G, Napoli A, Realfonzo R. Reliable design and optimization of SRP-, CFRP-, and GFRP-confined concrete: experimental validation and cost-effectiveness analysis. Mater Struct. 2025;58(10):350. doi:10.1617/s11527-025-02871-y.
35. Shah G, Das N, Nanthagopalan P. In-depth exploration of the behavior of UHPC in subzero conditions: static and dynamic loading scenarios. J Mater Civ Eng. 2026;38(1):04025491. doi:10.1061/jmcee7.mteng-20684.
36. Lyu J, Feng S. Investigation of bond shear behaviour of UHPC-NSC and damage prediction model under salt freeze-thaw environment. Eng Struct. 2025;330(1):119891. doi:10.1016/j.engstruct.2025.119891.